ACS APPLIED MATERIALS & INTERFACES

Research Article

www.acsami.org

Synthesis of a Highly Efficient BiOCl Single-Crystal Nanodisk Photocatalyst with Exposing {001} Facets

Xing Zhang,[†,‡] Xin-Bo Wang,[†] Li-Wei Wang,[†] Wei-Kang Wang,[†] Lu−Lu Long,[†] Wen-Wei Li,[†] and Han-Qing Yu*[,†,‡]

[†]Department of Chemistry, University of Science and Technology of China, Hefei, Anhui, China

[‡]Collaborative Innovation Center of Suzhou Nano Science and Technology, University of Science and Technology of China, Hefei, Anhui, China

Supporting Information

ABSTRACT: BiOCl is known as a highly efficient photocatalyst for degradation of pollutants. However, effective methods for fabricating BiOCl nanomaterials with well-defined facets are still lacking. In this work, a facile synthetic method was developed for the fabrication of BiOCl nanodisks with exposed {001} facets. The central feature of this approach was the use of water as the hydrolysis agent and ethylene glycol as the crystal growth inhibitor agent to tune the growth of BiOCl nanomaterial. With this approach, the size and shape of BiOCl nanostructures could be effectively tuned through adjusting the volume ratio of ethylene glycol/H_2O. In addition, the mechanism of the crystal growth in this fabrication process was elucidated. The as-prepared BiOCl nanodisks with exposed {001} facets exhibited an excellent photocatalytic activity towards Rhodamine B degradation under both ultraviolet and visible light irradiations. These findings shed light on the deep understanding of formation mechanisms of BiOCl nanodisks and provide an efficient and facile method for the synthesis of high active photocatalyst.

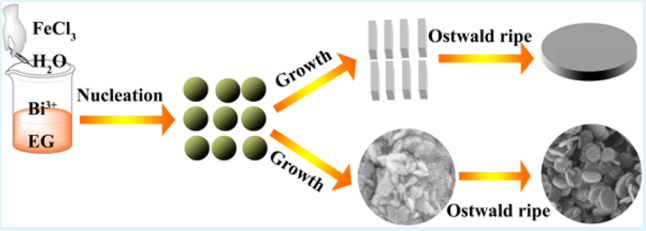

KEYWORDS: *BiOCl, degradation, facets, nanodisk, photocatalysis, visible light*

INTRODUCTION

Layered materials, such as graphene,[1] are promising materials for sensing,[2] catalysis,[3] manufacturing device,[4,5] solid-state lubricant,[6] and energy storage applications.[7] These materials possess two-dimensional (2D) crystals structure, high specific surface areas, and large fraction of uncoordinated surface atoms relative to the corresponding bulks. In parallel with the development of graphene-like materials, a complex ternary layer compound, BiOCl, has also been extensively investigated for one decade.[8−12] Recently, a facet-controlled fabrication of single-crystalline BiOCl semiconductors with well-defined morphology is attracting great interests.[12−17] It was found that the photocatalytic activity of these materials depended sensitively on the exposed surfaces with distinct crystal facets. A comparison among the photocatalytic activities of the BiOCl single-crystalline nanosheets with different exposed facets shows that the nanosheets with exposed {001} facets exhibited a higher activity for direct semiconductor photoexcitation degradation of pollutants under UV irradiation, but their counterpart with exposed {010} facets possessed a superior activity for indirect dye photosensitization degradation of pollutants under visible light irradiation.[12] In addition, it was demonstrated that ultrathin BiOCl nanosheets of {001} facets with an atomic-scale thickness for the increased surface vacancy associate possessed an enhanced adsorption capability and enabled effective separation of the electron-hole pairs.[16] Density functional theory calculations on the photocatalytic properties of BiOCl nanosheets with {001}, {110}, and {010} facets confirm that X-terminated (X = F, Cl, Br, and I) bulk-like {001} facets with clear boundary of $[Bi_2O_2]$ and halogen slabs had a high thermodynamic stability and efficient separation of photo-induced e^-−h^+ pairs.[18,19]

However, since Bi^{3+} ions are liable to hydrolysis in water solution, the synthesis of BiOCl nanostructure is usually conducted in solvent system, such as ethylene glycol (EG), diethylene glycol, triethylene glycol,[20−22] or in acid-assisted water system (e.g., citric acid and hydrochloric acid).[23−27] In these systems, three dimensional microspheres are usually obtained. For these microsphere morphologies, contaminants adsorbed on their surface reduce their catalytic activity. Thus, synthetic methods of highly active BiOCl catalysts are greatly needed. As aforementioned, 2D BiOCl nanomaterial with {001} facets has a high catalytic activity and layer-structured BiOCl could be readily grown into 2D nanostructure because of the inherent crystal growth tendency in water system. However, controlling of the hydrolysis of Bi^{3+} ions in water systems and obtaining uniform, well dispersed and high-purity 2D BiOCl are the main problem to be resolved. Therefore,

Received: February 19, 2014
Accepted: April 30, 2014
Published: May 5, 2014

   dx.doi.org/10.1021/am5010392 | ACS Appl. Mater. Interfaces 2014, 6, 7766−7772

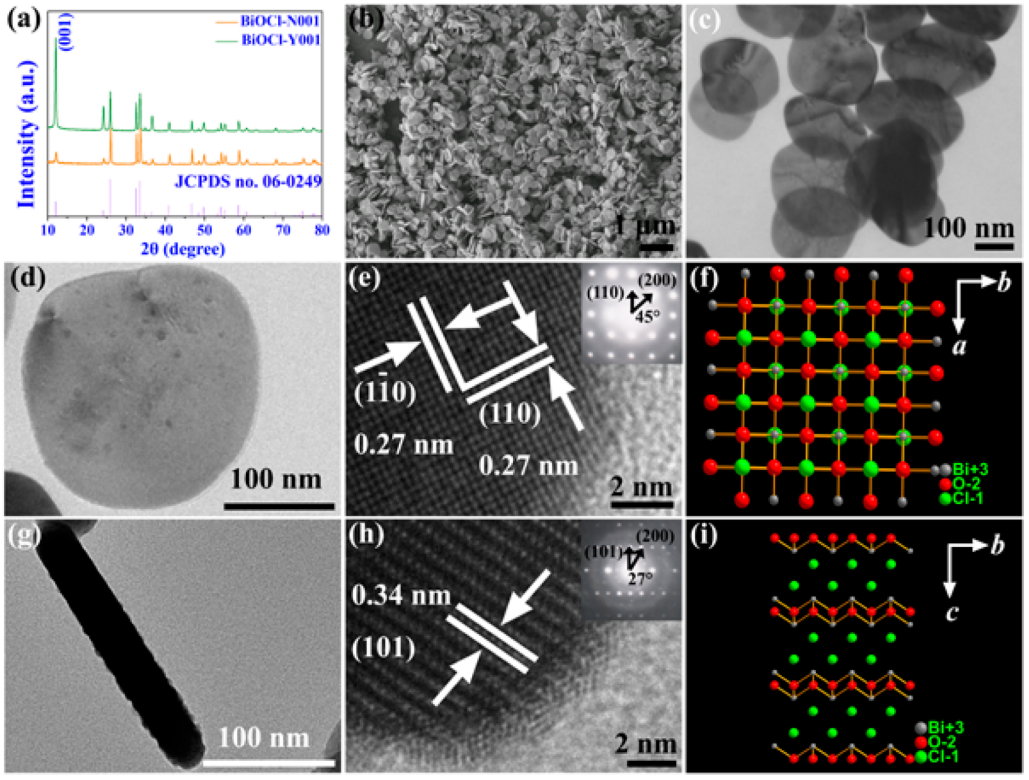

Figure 1. (a) XRD patterns of the BiOCl-N001 and BiOCl-Y001 nanodisks; (b) SEM image; (c) TEM image of the BiOCl-Y001 nanodisks; (d) TEM image of single BiOCl-Y001 nanodisk surface; (e) HRTEM image of the BiOCl-Y001 nanodisks surface and insert is the corresponding SAED; (f) the crystal structure of BiOCl of (001) orient; (g) TEM image of BiOCl nanodisk lateral; (h) HRTEM image of single BiOCl nanodisk lateral and insert is the corresponding SAED; and (i) the crystal structure of BiOCl of (100) orient.

effective methods for controlled synthesis of 2D BiOCl nanomaterials with {001} facets are highly desired.

In this work, in order to resolve the Bi^{3+} hydrolysis problem in water system and synthesize uniform and high-purity 2D BiOCl nanodisks with exposed {001} facets, we proposed a new facile approach through combining organic solvent and water, elucidated their formation mechanism in terms of crystal growth tendency, and demonstrated their high photocatalytic activity for pollutant degradation.

EXPERIMENTAL SECTION

Preparation of the 2D BiOCl-Y001 Nanodisks. All chemicals used in this work were of analytical grade and purchased from Shanghai Chemical Reagent Co., China.

In a typical procedure of the nanodisks preparation, 0.972 g $Bi(NO_3)_3{\cdot}5H_2O$ (2 mmol) was added into 15 mL EG. Under vigorous stirring and sonication for 10 min, the mixture was dispersed to form a homogeneous solution. In parallel, 0.541 g $FeCl_3{\cdot}6H_2O$ (2 mmol) was added into 15 mL distilled water under vigorous stirring for 5 min to form a homogeneous solution. Then, the above two solutions were mixed, and a white suspension was formed immediately. The white suspension was transferred into a 50 mL autoclave with a Teflon linear, which was heated at 160 °C for 12 h, and then naturally cooled to ambient temperature. The resulting solid powders were collected through centrifugation and washed with distilled water and absolute alcohol for several times to remove residual ions. The final products were then dried at 70 °C for 6 h prior to characterization.

Physicochemical Characterization of the Samples. The X-ray powder diffraction (XRD) patterns of the samples were obtained on a Philips X' Pert PRO SUPER diffractometer equipped with graphite monochromatized Cu Kα radiation (λ = 1.541874 Å). The scanning electron microscopy (SEM) images of the samples were taken with an X-650 scanning electron micro analyzer and a JSM-6700F field emission SEM (JEOL Co., Japan). The transmission electron microscopy (TEM) images of the samples were recorded on a TEM (H-7650, Hitachi Co., Japan), using an electron kinetic energy of 100 kV. The high-resolution transmission electron microscopy (HRTEM) images and selected area electron diffraction (SAED) patterns were taken on an HRTEM (2010, JEOL Co., Japan) at an acceleration voltage of 200 kV. The chemical compositions and the valence states of constituent elements were analyzed by X-ray photoelectron spectroscopy (XPS) (ESCALAB250, Thermo Fisher Inc., U.S.A.). The diffuse reflectance spectra (DRS) were measured using a UV/Vis spectrophotometer (Solid 3700, Shimadzu Co., Japan). The surface area was measured by the Brunauer–Emmett–Teller (BET) method with a Builder 4200 instrument (Tristar II 3020M, Micromeritics Co., U.S.A.).

Photocatalytic Measurements. The photocatalytic activity of the BiOCl nanodisks for the degradation of Rhodamine B (RhB) was evaluated using a UV light (λ = 254 nm) or 350 W Xe arc lamp with a 420 nm cutoff filter as the light source at ambient temperature. Before the tests, 0.02 g of BiOCl nanodisks as a photocatalyst was added into 30 mL aqueous solution containing 20 mg L^{-1} RhB, and stirred in dark for 30 min to ensure sufficient adsorption/desorption equilibrium. Then, under light irradiation and continuously magnetic stirring, samples were collected at given time intervals and the RhB concentration was measured with a UV–vis spectrometer (U-3310, Hitachi Co., Japan).

RESULTS AND DISCUSSION

Morphology and Microstructure of the BiOCl Nanodisks. Figure 1a shows the XRD patterns of the prepared BiOCl samples. The main diffraction peaks were identical to those of the tetragonal phase BiOCl (JCPDS card no. 06-0249). The (001) peak was much higher than the standard card, implying that the exposed surfaces of sample consisted of

dx.doi.org/10.1021/am5010392 | ACS Appl. Mater. Interfaces 2014, 6, 7766–7772

{001} facets (denote as BiOCl-Y001). The SEM images (Figure 1b) reveals that the sample possessed large-scale disk-like structures with diameter of 100−300 nm and thicknesses of 15−30 nm. The TEM images (Figure 1c) further confirms such a disk-like structure. The HRTEM image (Figure 1e), which was taken from the edge of the single nanodisk in Figure 1d, reveals a highly crystalline and clear lattice fringes projected along the [001] axis. The continuous lattice fringes with an interplanar lattice spacing of 0.27 nm and an angle of 90° matched well with the (110) atomic planes of the tetragonal BiOCl. The corresponding SAED pattern (insert in Figure 1e) indicates a single-crystalline nature of the BiOCl-Y001 nanodisk. The angle labelled in the SAED pattern was 45°, which is in agreement with the theoretical calculation of the angle between the (110) and (200) planes. The set of diffraction spots can be indexed as the [001] zone axis of tetragonal BiOCl.

Figure 1f shows the BiOCl [001] projection crystal structure. The HRTEM image (Figure 1h), which was taken from the tip of the single nanodisk in Figure 1g, also reveals a high crystallinity of the sample. The continuous lattice fringes with an interplanar lattice spacing of ∼0.34 nm matched well with the (101) atomic planes of the tetragonal BiOCl. The corresponding SAED pattern (insert in Figure 1h) also confirms the presence of single-crystalline BiOCl nanodisk. The angle labelled in the SAED pattern was 27°, which is in agreement with the theoretical calculation of the angle between the (101) and (200) planes. The set of diffraction spots could be indexed as the [010] zone axis of tetragonal BiOCl. Figure 1i shows the BiOCl [100] projection crystal structure.

XPS analysis was performed to explore the surface compositions and chemical states of the as-prepared BiOCl-Y001 nanodisks. From the full scan spectrum shown in Figure 2a, the peaks of Bi, O, Cl, and C elements could be identified.

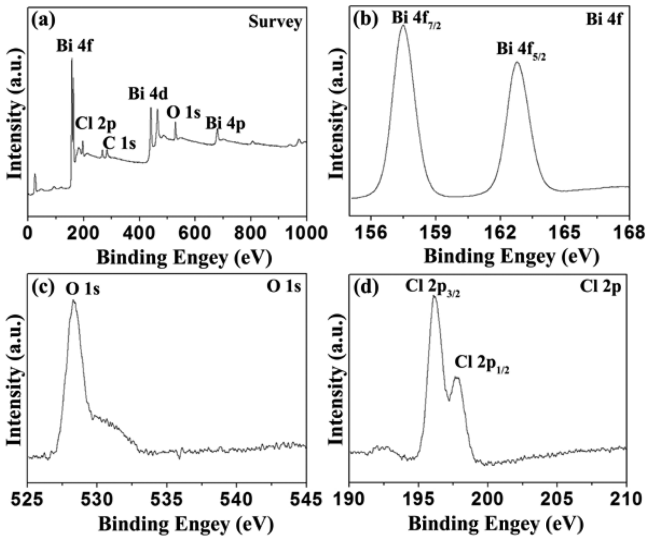

Figure 2. XPS spectra of (a) survey spectrum; (b) Bi 4f; (c) O 1s; and (d) Cl 2p for BiOCl-Y001 nanodisks.

The XPS spectra were corrected for specimen charging by referencing the C 1s peak at 284.60 eV. The Bi 4f XPS spectrum (Figure 2b) shows two main peaks with binding energies at 157.4 and 162.8 eV, corresponding to Bi $4f_{7/2}$ and Bi $4f_{5/2}$ of Bi^{3+}, respectively. The O 1s core level spectrum (Figure 2c) could be fitted well with the peak at 528.3 eV, which belongs to O^{2-} from a bismuth−oxygen bond in BiOCl. The Cl 2p XPS spectrum shows two major peaks with binding energies at 196.2 and 197.8 eV, corresponding to Cl $2p_{3/2}$ and Cl $2p_{1/2}$ of Cl^-, respectively (Figure 2d).[21,26] All the above results demonstrate that the formed nanostructures were composed of BiOCl.

Formation Mechanism of BiOCl Nanodisks and Key Factors Involved. In order to elucidate the formation mechanism of BiOCl nanodisks, the growth process was studied by analyzing the XRD patterns and SEM images of the products at various reaction stages. As shown in Figure 1a and Supporting Information (SI) Figure S1, the (001) diffraction peak was enhanced over time, indicating that the BiOCl was formed under ambient temperature. Figure 3a illustrates the

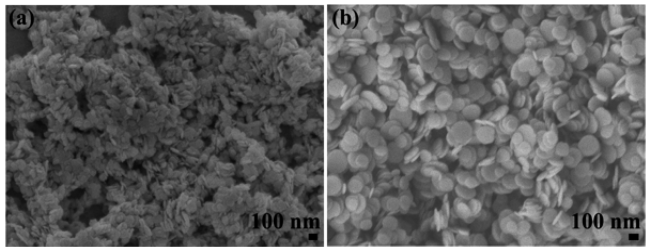

Figure 3. Growth of the BiOCl nanocrystal at different reaction steps: (a) the initial of white suspension; (b) 160 °C for 1 h.

SEM image of the sample at the initial reaction stage, from which only a plate-like BiOCl nanocrystal was observed. The plate-like BiOCl nanocrystals were irregular and agminated with a size of 100−200 nm. Figure 3b shows that BiOCl nanocrystals with disk-like structure and good dispersion were formed (denoted as BiOCl-N001) after 1-h reaction, and the size of the BiOCl-N001 nanodisks was ∼200−300 nm. The gradual increase in BiOCl size was an Ostwald ripening process. After 3-h reaction, the morphology of the BiOCl nanocrystals was still disk-like (SI Figure S2). These results imply that the BiOCl structure was inter-grown with $[Bi_2O_2]$ slabs interleaved by double slabs of Cl atoms. This could be used to explain why the oxyhalide compounds could easily form 2D laminar structure.

Our results are different from the reports using organic solvent method only, with which three-dimensional microspheres were usually obtained.[20] Such a difference might be attributed to the only existence of EG solvent in their study, which acted as a crystal growth inhibitor. As a consequence, the lamellar crystals easily generated curvature and were developed into flower-like morphology.[10,28,29] On the other hand, with the dose of water in our study, the crystal growth inhibitory effect of EG became diminished, so that the growth of the microstructure was turned into 2D laminar structure with well dispersion, rather than three-dimensional microspheres.

To validate the above assumption, comparative experiments were carried out and the resulting morphologies were observed by SEM. Without the dose of water, the product was almost entirely composed of a large quantity of uniform BiOCl microspheres with an average diameter of ∼1 μm (Figure 4a). The microspheres had flowerlike shapes, which were organized from numerous thin nanoplates with a thickness of ∼24 nm in an interwoven arrangement. However, when the volume ratio of EG/H_2O was decreased to 28:2, microplates (Figure 4b) with a diameter of ∼1 μm were formed, which were self-assembled by nanoplates with a thickness of ∼20 nm (insert in

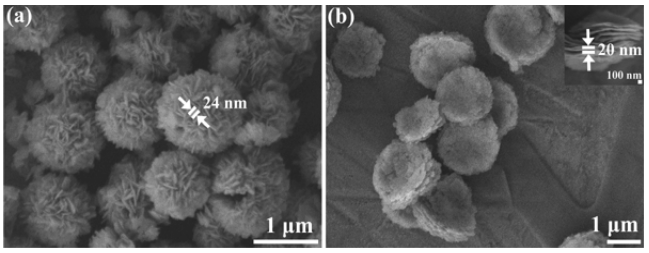

Figure 4. SEM images of the BiOCl prepared at 160 °C for 12 h in different volume ratios of EG/H_2O: (a) 30:0; (b) 28:2.

Figure 4b). With a further decrease in volume ratio of EG/H_2O to 20:10, the products were almost all nanoplates with a size of ~100 nm and a thickness of ~20 nm (SI Figure S3). When the volume ratio of EG/H_2O was decreased to 0:30, the sample exhibited large-scale plate-like structures with a diameter of 200−5000 nm (SI Figure S4). These results demonstrate that the morphologies of BiOCl could be effectively tuned by adjusting the volume ratio of EG/H_2O.

Additional experiments were conducted in order to examine whether the metal ions also played an important role in controlling the size and shape growth of BiOCl nanomaterials. The corresponding products were examined by XRD and SEM, as shown in Figure 5 and SI Figure S5. All the products were

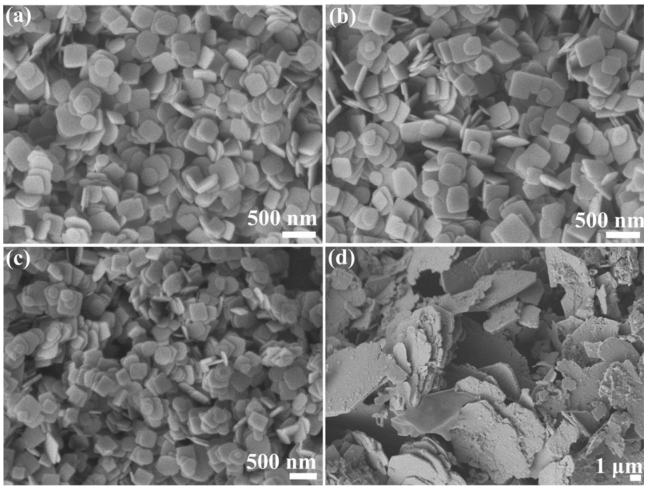

Figure 5. SEM images of the BiOCl samples grown from the metal chloride solutions: (a) $CoCl_2$; (b) $NiCl_2$; (c) $ZnCl_2$; (d) $SnCl_2$.

obtained under the same conditions as detailed above. When 3 mmol $CoCl_2$, $NiCl_2$, and $ZnCl_2$ were used to replace the $FeCl_3$, with the other constant conditions, the size of the synthesized 2D square nanoplates was about 500 nm (Figure 5a−c). When 3 mmol $SnCl_2$ was used instead, the dominant products were 2D microplates with a size of 1−15 μm (Figure 5d). The corresponding XRD patterns in SI Figure S5 indicate that all the 2D BiOCl nanostructures were (001) planes orient. These results show that the species of metal ions also contributed to the tuning of the BiOCl size and shape but did not affect the 2D plate-like structure.

The formation mechanism of the BiOCl-Y001 nanodisks is illustrated in Scheme 1a: (1) rapid nucleation at the initial stage; (2) nucleation growth into the plate-like BiOCl nanocrystals; and (3) Ostwald ripening growth of the plate-like BiOCl nanocrystal into the 2D BiOCl nanodisks. The size and shape of BiOCl could be tuned through adjusting the

Scheme 1. Tuning Size and Shape of BiOCl

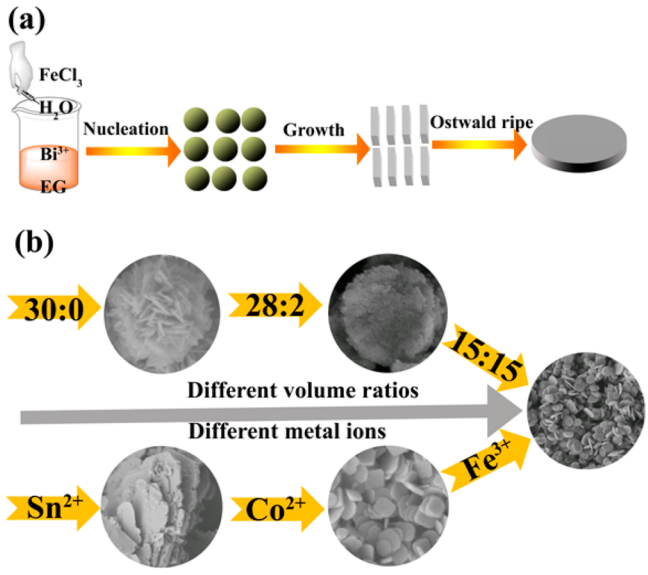

volume ratio of EG/H_2O and changing the metal chlorides, as illustrated in Scheme 1b.

Furthermore, application of this approach to the synthesis of other Bi-based oxyhalides was also demonstrated. In the presence of 6 mmol KBr or KI, 2D square-like BiOBr and BiOI with a diameter in micrometer scale were formed (Figure 6a,

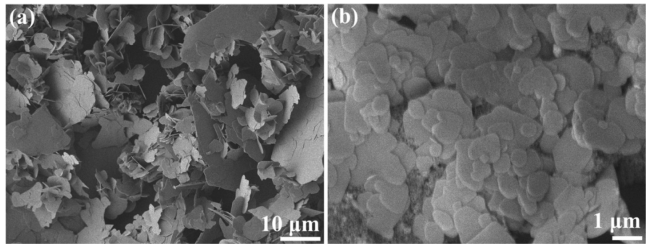

Figure 6. SEM images of the samples: (a) BiOBr; (b) BiOI.

b). This result shows that the mixed-solvent system used in this study was effective for the synthesis of 2D Bi-based oxyhalides nanostructures. Therefore, an efficient and facile approach for the synthesis of 2D bismuth oxyhalide nanomatrials with exposed {001} facets was established.

Optical Absorption Properties and BET Surface Areas of the BiOCl Nanodisks. The photocatalytic activity of a semiconductor is closely related to its energy band structure feature. Figure 7 shows the UV−vis diffuse reflectance spectra of the BiOCl-Y001 and BiOCl-N001 nanodisks. It is known that the optical absorption of a crystalline indirect semiconductor near the band edge follows the formula $(\alpha h\nu)^{1/2} = B(h\nu - E_g)$, where α, $h\nu$, E_g, and B are the absorption coefficient, photon energy, band gap and a constant, respectively.[21] The absorption edges of the BiOCl-Y001 and BiOCl-N001 nanodisks are 399 and 377 nm and the estimated band gap energies of the as-obtained were about 3.11 and 3.29 eV from the absorption onsets, respectively. The results indicate that the BiOCl-Y001 had a narrower band gap, which might be attributed to its morphology, size, and specific structure.

The BET specific surface area of the synthesized BiOCl nanodisks was evaluated using the nitrogen adsorption-

dx.doi.org/10.1021/am5010392 | ACS Appl. Mater. Interfaces 2014, 6, 7766−7772

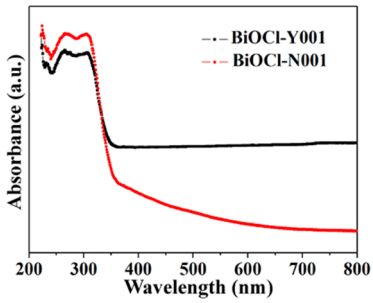

Figure 7. UV–vis diffuse reflectance spectra of BiOCl-Y001 and BiOCl-N001 nanodisks.

desorption method. The nitrogen adsorption-desorption isotherms of the BiOCl-Y001 and BiOCl-N001nanodisk are illustrated in Figure 8, whereas the corresponding pore-size

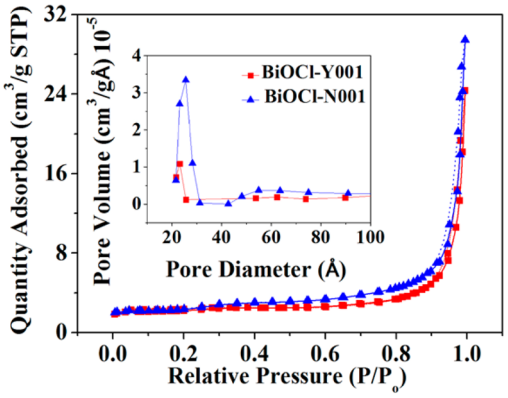

Figure 8. Nitrogen adsorption–desorption isotherm plot and corresponding pore-size distribution (insert) of the as-prepared BiOCl-Y001 and BiOCl-N001nanodisks.

distributions are shown in the insets of Figure 8. The BET surface areas of the BiOCl-Y001 and BiOCl-N001nanodisks calculated from the results of N_2 adsorption were 7.6 and 8.0 m^2/g, respectively. The BiOCl-Y001 nanodisks had a smaller surface area than the BiOCl-N001 nanodisks.

Photocatalytic Activity of the BiOCl Nanodisks. To explore the photocatalytic capacity of the BiOCl nanodisks and identify the relationship between the exposed crystallographic facets and the photocatalytic activity, utilization of both the prepared BiOCl-Y001 and BiOCl-N001 nanodisks for the photocatalytic degradation of RhB as the target pollutant was tested.

The RhB evolution of UV–vis spectra over time with the BiOCl-Y001 nanodisks is illustrated in Figure 9a. The intensity of absorption peak at 552 nm decreased drastically over time, and completely disappeared after 120 min. To explore the photocatalytic activity of the nanodisks with {001} facets, a direct photolysis of RhB by the BiOCl-N001 nanodisks was tested under identical conditions. Figure 9b displays the temporal evolution of the spectra in the photodegradation of RhB under UV light irradiation, whereas Figure 9c shows the variation in RhB concentrations (C/C_0) with different photocatalysts over time. It was observed that the RhB concentration remained unchanged over time in the absence of catalysts, while the photocatalytic degradation efficiency after 120 min was only 60% for the BiOCl-N001 nanodisks,

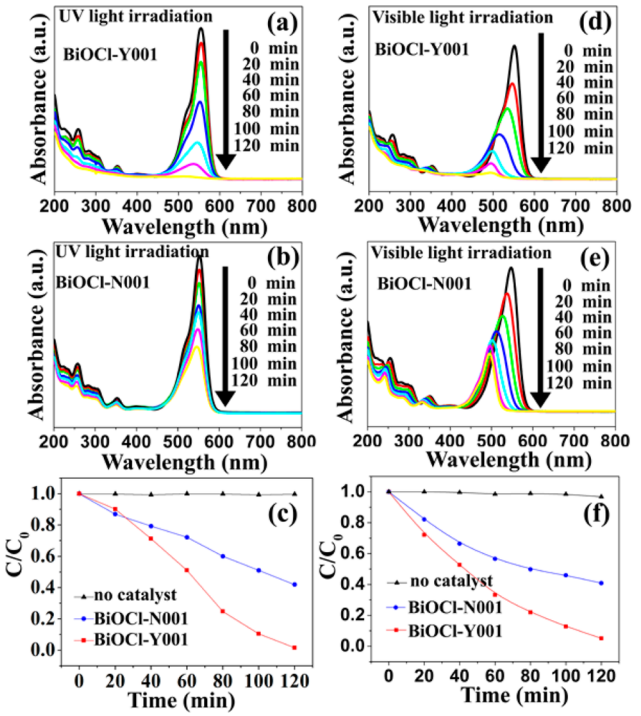

Figure 9. (a, b) Photodecomposition of RhB with the BiOCl samples under UV irradiation; (d, e) photodecomposition of RhB with the BiOCl samples under visible light irradiation; (c, f) comparison of photodecomposition of RhB *vs* time by the BiOCl-Y001 nanodisks and the BiOCl-N001 nanodisks under UV and visible light irradiation.

indicating that the BiOCl-Y001 nanodisks exhibited a higher photocatalytic activity compared to the BiOCl-N001 nanodisks.

The photocatalytic degradation of dyes on semiconductors can be achieved through direct semiconductor photoexcitation or indirect dye photosensitization. These two photocatalytic pathways respond differently to light with different wavelengths. To find out the photocatalytic pathway here, the RhB degradation performance by both the BiOCl-Y001 and BiOCl-N001 nanodisks under visible light irradiation was also investigated. As shown in Figure 9d and e, the photocatalytic reactivity of the BiOCl-Y001 nanodisks was much higher than that of the BiOCl-N001 nanodisks under visible light irradiation.

To evaluate the {001} facets stability of BiOCl-Y001 nanodisks after degradation of RhB under UV light and visible light irradiations, cycle experiments of the photocatalyst were conducted. The photocatalyst samples after the cycle experiments were disk-like structure (SI Figure S6a and d). The HRTEM images in SI Figure S6b and e display a highly crystalline and clear lattice fringes projected along the [001] axis. The continuous lattice fringes with an interplanar lattice spacing of 0.27 nm and an angle of 90° matched the (110) atomic planes of the tetragonal BiOCl well. The corresponding SAED patterns in SI Figure S6c and f indicate that the single-crystalline nature of the BiOCl-Y001 nanodisk was maintained after the recycle experiments. The angle labelled in the SAED pattern is 45°, which is in agreement with the theoretical calculation of the angle between the (110) and (200) planes. All these results show that there was no obvious change in the tetragonal phase of the BiOCl-Y001 nanodisks after photocatalytic degradation of RhB under UV and visible light irradiations.

dx.doi.org/10.1021/am5010392 | ACS Appl. Mater. Interfaces 2014, 6, 7766–7772

On the basis of the above results, both direct semiconductor photoexcitation and indirect dye photosensitization were catalyzed by the BiOCl-Y001 nanodisks. Interestingly, although the BiOCl-Y001 nanodisks had a smaller specific surface area (7.6 m^2/g) less than the BiOCl-N001 nanodisks (8.0 m^2/g), their overall activity for RhB photodegradation was higher than that of the latter, suggesting that the overall photocatalytic activity of the BiOCl nanodisks is more directly related to their surface structure rather than the specific surface area.[30] The self-induced internal electric fields of the 2D nanostructure could induce more efficient photoinduced charge separation and transfer along the [001] direction in the BiOCl-Y001 nanodisks than the BiOCl-N001 nanodisks.[12,31,32] The BiOCl-Y001 nanodisks could prevent the recombination of photogenerated electron−hole pairs to increase the photocatalytic degradation of RhB. Therefore, a synergistic effect between the surface properties and suitable internal electric fields might be responsible for the higher photoreactivity of the BiOCl-Y001 nanodisks for both direct photoexcitation under ultraviolet light and indirect dye photosensitization degradation of RhB under visible light irradiation.

CONCLUSIONS

In this work, BiOCl nanodisks with exposed (001) were synthesized by using a new facile approach with a mixture of solvent EG and water. A variation of the EG/water volume ratio or the type of metal ions could be used to tune the shapes of BiOCl nanostructure. The formation of the BiOCl-Y001 nanodisks was a three-step process: the rapid nucleation at the initial stage and later growth into plate-like nanocrystals, followed by the Ostwald ripening growth of the plate-like BiOCl nanocrystals into the 2D BiOCl nanostructures. The prepared BiOCl-Y001 nanodisks exhibited a higher photocatalytic activity than the BiOCl-N001 nanodisks for both direct photoexcitation under ultraviolet light and indirect dye photosensitization degradation of RhB under visible light irradiation. These findings shed light on the BiOCl growth process and also might provide an efficient method for synthesizing other highly efficient nano-sized photocatalysts.

ASSOCIATED CONTENT

Supporting Information

XRD patterns of the BiOCl samples; SEM image of the BiOCl samples prepared at the volume EG/H_2O ratios of 20:10 and 0:30; TEM image of the BiOCl samples which were obtained after being heated at 160 °C for 3 h. HRTEM images of BiOCl-Y001 nanodisks after the recycle experiments under UV light and visible light irradiations. This material is available free of charge via the Internet at http://pubs.acs.org/.

AUTHOR INFORMATION

Corresponding Author

*Fax: +86-551-63601592. E-mail: hqyu@ustc.edu.cn.

Notes

The authors declare no competing financial interest.

ACKNOWLEDGMENTS

This work is supported by the National Basic Research Program of China (2011CB933700) and the Program for Changjiang Scholars and Innovative Research Team in University of the Ministry of Education of China and the Open Project of State Key Laboratory of Urban Water Resource and Environment (No. QA201402).

REFERENCES

(1) Novoselov, K. S.; Geim, A. K.; Morozov, S.; Jiang, D.; Zhang, Y.; Dubonos, S.; Grigorieva, I.; Firsov, A. Electric Field Effect in Atomically Thin Carbon Films. *Science* **2004**, *306*, 666−669.

(2) Li, H.; Yin, Z.; He, Q.; Li, H.; Huang, X.; Lu, G.; Fam, D. W. H.; Tok, A. I. Y.; Zhang, Q.; Zhang, H. Fabrication of Single-and Multilayer MoS_2 Film-Based Field-Effect Transistors for Sensing NO at Room Temperature. *Small* **2012**, *8*, 63−67.

(3) Li, Y.; Wang, H.; Xie, L.; Liang, Y.; Hong, G.; Dai, H. MoS_2 Nanoparticles Grown on Graphene: An Advanced Catalyst for the Hydrogen Evolution Reaction. *J. Am. Chem. Soc.* **2011**, *133*, 7296−7299.

(4) Ci, L.; Song, L.; Jin, C.; Jariwala, D.; Wu, D.; Li, Y.; Srivastava, A.; Wang, Z.; Storr, K.; Balicas, L. Atomic Layers of Hybridized Boron Nitride and Graphene Domains. *Nat. Mater.* **2010**, *9*, 430−435.

(5) Radisavljevic, B.; Radenovic, A.; Brivio, J.; Giacometti, V.; Kis, A. Single-Layer MoS_2 Transistors. *Nat. Nanotechnol.* **2011**, *6*, 147−150.

(6) Ramakrishna Matte, H.; Gomathi, A.; Manna, A. K.; Late, D. J.; Datta, R.; Pati, S. K.; Rao, C. MoS_2 and WS_2 Analogues of Graphene. *Angew. Chem.* **2010**, *122*, 4153−4156.

(7) Xiao, J.; Choi, D.; Cosimbescu, L.; Koech, P.; Liu, J.; Lemmon, J. P. Exfoliated MoS_2 Nanocomposite as An Anode Material for Lithium Ion Batteries. *Chem. Mater.* **2010**, *22*, 4522−4524.

(8) Deng, H.; Wang, J.; Peng, Q.; Wang, X.; Li, Y. Controlled Hydrothermal Synthesis of Bismuth Oxyhalide Nanobelts and Nanotubes. *Chem.—Eur. J.* **2005**, *11*, 6519−6524.

(9) Henle, J.; Kaskel, S. Preparation of Photochromic Transparent BiOX (X = Cl, I)/PLA Nanocomposite Materials via Microemulsion Polymerization. *J. Mater. Chem.* **2007**, *17*, 4964−4971.

(10) Peng, H.; Chan, C. K.; Meister, S.; Zhang, X. F.; Cui, Y. Shape Evolution of Layer-Structured Bismuth Oxychloride Nanostructures via Low-Temperature Chemical Vapor Transport. *Chem. Mater.* **2008**, *21*, 247−252.

(11) Chang, X.; Huang, J.; Cheng, C.; Sui, Q.; Sha, W.; Ji, G.; Deng, S.; Yu, G. BiOX (X = Cl, Br, I) Photocatalysts Prepared Using $NaBiO_3$ As the Bi Source: Characterization and Catalytic Performance. *Catal. Commun.* **2010**, *11*, 460−464.

(12) Jiang, J.; Zhao, K.; Xiao, X.; Zhang, L. Synthesis and Facet-Dependent Photoreactivity of BiOCl Single-Crystalline Nanosheets. *J. Am. Chem. Soc.* **2012**, *134*, 4473−4476.

(13) Weng, S.; Pei, Z.; Zheng, Z.; Hu, J.; Liu, P. Exciton-Free, Nonsensitized Degradation of 2-Naphthol by Facet-Dependent BiOCl under Visible Light: Novel Evidence of Surface-State Photocatalysis. *ACS Appl. Mater. Interfaces* **2013**, *5*, 12380−12386.

(14) Ye, L.; Zan, L.; Tian, L.; Peng, T.; Zhang, J. The {001} Facets-Dependent High Photoactivity of BiOCl Nanosheets. *Chem. Commun.* **2011**, *47*, 6951−6953.

(15) Xu, Y.; Xu, S.; Wang, S.; Zhang, Y.; Li, G. Citric Acid Modulated Electrochemical Synthesis and Photocatalytic Behavior of BiOCl Nanoplates with Exposed {001} Facets. *Dalton Trans.* **2013**, *43*, 479−485.

(16) Guan, M.; Xiao, C.; Zhang, J.; Fan, S.; An, R.; Cheng, Q.; Xie, J.; Zhou, M.; Ye, B.; Xie, Y. Vacancy Associates Promoting Solar-Driven Photocatalytic Activity of Ultrathin Bismuth Oxychloride Nanosheets. *J. Am. Chem. Soc.* **2013**, *135*, 10411−10417.

(17) Zhao, K.; Zhang, L.; Wang, J.; Li, Q.; He, W.; Yin, J. J. Surface Structure-Dependent Molecular Oxygen Activation of BiOCl Single-Crystalline Nanosheets. *J. Am. Chem. Soc.* **2013**, *135*, 15750−15753.

(18) Zhang, H.; Liu, L.; Zhou, Z. First-Principles Studies on Facet-Dependent Photocatalytic Properties of Bismuth Oxyhalides (BiOXs). *RSC Adv.* **2012**, *2*, 9224−9229.

(19) Zhang, X.; Zhao, L.; Fan, C.; Liang, Z.; Han, P. First-Principles Investigation of Impurity Concentration Influence on Bonding Behavior, Electronic Structure, and Visible Light Absorption for Mn-doped BiOCl Photocatalyst. *Physica B: Condensed Matter* **2012**, *407*, 4416−4424.

(20) Xiong, J.; Cheng, G.; Qin, F.; Wang, R.; Sun, H.; Chen, R. Tunable BiOCl Hierarchical Nanostructures for High-Efficient Photocatalysis under Visible Light Irradiation. *Chem. Eng. J.* **2013**, *220*, 228−236.
(21) Cheng, G.; Xiong, J.; Stadler, F. J. Facile Template-Free and Fast Refluxing Synthesis of 3D Desertrose-like BiOCl Nanoarchitectures with Superior Photocatalytic Activity. *New J. Chem.* **2013**, *37*, 3207−3213.
(22) Liu, Q.-C.; Ma, D.-K.; Hu, Y.-Y.; Zeng, Y.-W.; Huang, S.-M. Various Bismuth Oxyiodide Hierarchical Architectures: Alcohothermal-Controlled Synthesis, Photocatalytic Activities, and Adsorption Capabilities for Phosphate in Water. *ACS Appl. Mater. Interfaces* **2013**, *5*, 11927−11934.
(23) Gnayem, H.; Sasson, Y. Hierarchical Nanostructured 3D Flowerlike $BiOCl_xBr_{1-x}$ Semiconductors with Exceptional Visible Light Photocatalytic Activity. *ACS Catal.* **2013**, *3*, 186−191.
(24) Zhang, K.; Liang, J.; Wang, S.; Liu, J.; Ren, K.; Zheng, X.; Luo, H.; Peng, Y.; Zou, X.; Bo, X. BiOCl Sub-microcrystals Induced by Citric Acid and Their High Photocatalytic Activities. *Cryst. Growth Des.* **2012**, *12*, 793−803.
(25) Zhang, W.; Zhang, Q.; Dong, F. Visible Light Photocatalytic Removal of NO in Air over BiOX (X = Cl, Br, I) Single-Crystal Nanoplates Prepared at Room Temperature. *Ind. Eng. Chem. Res.* **2013**, *52*, 6740−6746.
(26) Peng, S.; Li, L.; Zhu, P.; Wu, Y.; Srinivasan, M.; Mhaisalkar, S. G.; Ramakrishna, S.; Yan, Q. Controlled Synthesis of BiOCl Hierarchical Self-Assemblies with Highly Efficient Photocatalytic Properties. *Chem.—Asian J.* **2013**, *8*, 258−268.
(27) Biswas, A.; Das, R.; Dey, C.; Banerjee, R.; Poddar, P. Ligand-Free One-Step Synthesis of {001} Faceted Semiconducting BiOCl Single Crystals and Their Photocatalytic Activity. *Cryst. Growth Des.* **2013**, *14*, 236−239.
(28) Zhang, X.; Qian, Y.; Zhu, Y.; Tang, K. Synthesis of Mn_2O_3 Nanomaterials with Controllable Porosity and Thickness for Enhanced Lithium-ion Batteries Performance. *Nanoscale* **2014**, *6*, 1725−1731.
(29) Xiong, S.; Yuan, C.; Zhang, X.; Xi, B.; Qian, Y. Controllable Synthesis of Mesoporous Co_3O_4 Nanostructures with Tunable Morphology for Application in Supercapacitors. *Chem.—Eur. J.* **2009**, *15*, 5320−5326.
(30) Xi, G.; Ye, J. Synthesis of Bismuth Vanadate Nanoplates with Exposed {001} Facets and Enhanced Visible-Light Photocatalytic Properties. *Chem. Commun.* **2010**, *46*, 1893−1895.
(31) Zhang, X.; Ai, Z.; Jia, F.; Zhang, L. Generalized One-Pot Synthesis, Characterization, and Photocatalytic Activity of Hierarchical BiOX (X = Cl, Br, I) Nanoplate Microspheres. *J. Phys. Chem. C* **2008**, *112*, 747−753.
(32) Xiao, X.; Liu, C.; Hu, R.; Zuo, X.; Nan, J.; Li, L.; Wang, L. Oxygen-Rich Bismuth Oxyhalides: Generalized One-Pot Synthesis, Band Structures and Visible-Light Photocatalytic Properties. *J. Mater. Chem.* **2012**, *22*, 22840−22843.